IET Optoelectronics

Research Article

IET Journals
The Institution of Engineering and Technology

Performance evaluation of asynchronous multi-carrier code division multiple access for next-generation long-reach fibre optic access networks

ISSN 1751-8768
Received on 25th August 2014
Revised on 18th February 2015
Accepted on 19th March 2015
doi: 10.1049/iet-opt.2014.0092
www.ietdl.org

Morteza H. Shoreh ✉, *Hamzeh Beyranvand*, *Jawad A. Salehi*

Optical Networks Research Laboratory (ONRL), Sharif University of Technology, Tehran, Iran
✉ *E-mail: m.h.shoreh@gmail.com*

Abstract: In this study, the authors evaluate the performance of asynchronous optical multi-carrier code division multiple access (MC-CDMA) for intensity modulated/direct detection systems to be used in next-generation optical access networks. The proposed system employs Gold sequence in frequency-domain to provide asynchronous resource sharing. In long-reach passive optical networks, fibre impairments degradation to the performance of ordinary optical CDMA can be avoided by frequency-domain digital compensation methods in the proposed MC-CDMA. In comparison with orthogonal frequency division multiple access, peak-to-average power ratio in the proposed MC-CDMA is reduced and asynchronous resource sharing is achieved. The performance of the proposed optical MC-CDMA system is analytically evaluated by driving closed-form equations for signal-to-interference plus noise ratio and bit error rate (BER) performances. Furthermore, the simulation results are provided in terms of BER against signal-to-noise ratio in one case and the number of users in another, conditioned on the modulation levels. Finally, the analytical formulation of BER is verified with the help of simulation results.

1 Introduction

Optical orthogonal frequency division multiplexing (OFDM) has been a promising candidate for future optical access networks [1]. This is caused by easy compensation of both chromatic and polarisation mode dispersion, spectral efficiency, adaptation to efficient channel estimation/equalisation, resilience to dominant linear impairments in fibre and compatibility with digital implementation [2–4]. Fast Fourier transform (FFT)-based implementation also enables a straightforward adaptation of the modulation formats on each OFDM subcarrier [5]. OFDM has a major advantage of transferring transceivers complexity to the digital domain [6]. For example, in OFDM-based implementation any frequency-dependent phase rotation can be compensated with acceptable cost utilising digital part of the receiver [7, 8].

Despite being new in optical communications systems, results show that OFDM can be a promising transmission technique; therefore any method proposed for wide spread use in future optical networks should be compatible with its intrinsic properties. In an optical OFDM access network, depending on the required bandwidth of an optical network unit (ONU), a number of subcarriers are assigned to that ONU as a means of resource sharing in passive optical network (PON) and it holds many advantages over other proposed methods such as speed, flexibility and cost efficiency [9–12]. However, a disadvantage of orthogonal frequency division multiple access, in case of not using controlling signals, is the reduction of spectral efficiency when some ONUs are inactive. This disadvantage arises since a predetermined frequency assignment to each device is used such that other devices cannot use the allocated spectrum and they cannot work in an asynchronous manner such as in up-link data transferring [13]. Hence, designing a more flexible resource sharing technique is an essential challenge.

One may think, such applications could be handled based on code division multiple access (CDMA) where users share the same time and spectrum but vary in code domain [14]. In general, CDMA provides the users the efficient utilisation of the available bandwidth since users are separated on code domain utilising all spectrum and time jointly [14]. For example, when the number of users is low the active users can use higher modulation levels to increase bit rate in order to use the channel more efficiently [15]. Moreover, higher security and flexibility have made CDMA a wise choice for PONs [16].

However, a drawback of the conventional optical CDMA is its low spectral efficiency in comparison with OFDM-based systems. In optical CDMA unipolar nature of light intensity requires especial unipolar CDMA codes. Since there is no negative sign to cancel the positive chips in cross-correlation calculation, these codes are sparse. This sparsity results in reduction of the spectral efficiency in the unipolar codes, referred as optical orthogonal codes in technical literature [17]. In [18], MC-CDMA has been experimentally demonstrated for the PON architecture. MC-CDMA is a combination of CDMA and OFDM techniques and exploits advantages of both of them [19]. In fact, MC-CDMA uses an OFDM-based transmitter and receiver to multiply the code on frequency domain and takes advantages of the dense subcarrier spacing of OFDM. By allocating coded subcarriers, MC-CDMA is able to support asynchronous bandwidth sharing, which is the main benefit of CDMA. Multiplying the code in frequency domain causes the code to be bipolar; hence, ordinary CDMA code sequences such as Walsh and gold can be used to encode OFDM subcarriers in frequency domain. It is worth mentioning that with the recent advances in digital signal processors, the final speed is not restricted by the processing speed of the electronic hardware anymore, devices such as the digital-to-analogue converter (DACs) limits the speed, thus the obtained spectral efficiency improvement overwhelm the increased computational complexity. Furthermore, easier frequency-domain equalisation is another benefit of MC-CDMA highlighting its benefits for next-generation long-reach access network.

In MC-CDMA technique, signal is spread in time domain so that the effective instantaneous power of the transmitted signal is reduced. This causes the radio-frequency and optical system to work on linear regions of operational amplifiers, hence, decreasing

its complexity and cost. Moreover, MC-CDMA has the ability to match the transmitted spectrum with the channel characteristic, causing easier use of pre-compensation methods, contrary to complex techniques such as time-domain pulse shaping in conventional optical CDMA systems [20].

Another advantage of the proposed MC-CDMA is its low peak-to-average power ratio (PAPR) in comparison with conventional OFDM systems [21]. In MC-CDMA technique, PAPR of the transmitted signal can be reduced further by carefully selecting low PAPR codes. Furthermore, in this method to increase a particular user's bit rate, more than one code can be assigned to that single user. In such a scenario, the codes assigned to a user work synchronously which can result in bit error rate (BER) performance improvement. This is due to the fact that in asynchronous system, BER performance is usually worst than synchronous counterpart [22]. MC-CDMA has been proposed and used in wireless access networks in recent years [23–27]. The MC-CDMA PON system has been experimentally demonstrated in [18]; however, to the best of our knowledge, this is the first paper that formulates and evaluates the performance of MC-CDMA system in fibre optic long-reach access networks.

The rest of this paper is organised as follows. In Section 2, the system model used in this paper is introduced. In Section 3, the concept of MC-CDMA and its performance evaluation are discussed. PAPR comparison with OFDM is done and PAPR reduction techniques are proposed in Section 4. Section 5 briefly describes the details of simulation employed to examine the proposed method and the provided results. Finally, Section 6 summarises the results and draws the conclusion.

2 System model

Conceptional block diagram of the MC-CDMA system is presented in Fig. 1. The data of each user are mapped to quadrature amplitude modulation (QAM) signal and then encoded with chip sequences of length N. The codes are applied on OFDM subcarriers via using serial-to-parallel converter and then the inverse FFT (IFFT) block, generating N equally spaced subcarriers at its output. After adding cyclic prefix (CP), the data are serialised in time domain. Finally, the DAC converts the data to analogue signal, which is filtered with single-side-band (SSB) filter and then fed to the Mach–Zehnder modulator (MZM). This optical signal goes through up to 80 km standard single mode fibre (SSMF) and other users' interference is added to it.

At the receiver, a simple photo-detector converts the received optical signal to electric domain where the reverse processes and equalisation are performed. Since the system uses OFDM-based transceiver, each output of the receiver FFT is a narrow-band signal which can be equalised by multiplying a simple complex constant. Hence by putting the equaliser just after the FFT block and before serialising the data we use simplified OFDM-based equaliser that shows another benefit of using OFDM-based systems. As represented by Fig. 1, a synchronisation loop is used to adjust the receiver FFT timing window to perfectly synchronise the desired user. It is worthy to note to mention that the equaliser in this structure is a memory-less block that multiplies each input (subcarrier) by a complex number. The data of the desired user are detected by correlating the output of the equaliser with the user's signature sequence, which is because of the low cross-correlation between each pair of signature sequences.

In this paper, the code length is chosen the same as the accessible FFT subcarriers and each QAM signal is multiplied to the user code to produce the entire data of a user in one OFDM symbol. Other users' signals go through the same procedure, and then will be added to this signal at any point of the optical link. Gold sequence codes are used, which give the system the ability to support asynchronous users in a shared medium. Therefore this demonstration is suitable for any of the down-link, up-link and peer-to-peer communication scenarios used in optical access networks. The proposed MC-CDMA scheme is especially beneficial in overcoming the challenges caused by the asynchronous and bursty nature of up-link traffic.

Fig. 2 schematically represents the coding and decoding processes of the MC-CDMA signal in frequency domain. First, the CDMA code is multiplied with OFDM subcarriers to produce the coded subcarriers represented in Fig. 2*b*. After considering all users transmitting their coded signals, the multiuser signal that should be dealt with at the receiver is depicted in Fig. 2*c*. Finally, by multiplying the code in frequency domain and considering the FFT and match filter of the receiver, the signal represented by Fig. 2*d* is achieved. Now, the desired user's data can be extracted considering all chips. The extracted signal is proportional to the QAM constellation points of the transmitted data of this user.

3 MC-CDMA performance evaluation

In MC-CDMA, each data symbol is transmitted over N narrow-band subcarriers. Multiple access is achieved with different users transmitting at the same set of subcarriers but using spreading codes that are orthogonal to each other. To have real data at the output of the transmitter IFFT, after the serial-to-parallel converter at the transmitter, $N/2-1$ subcarriers are used for modulation of the data which in this case is the output of the CDMA decoder and two subcarriers are set to zero for dc handling; in the rest of the IFFT inputs the conjugate of the first $N/2-1$ inputs are used. This method which is called Hermitian symmetry and cause the output of the IFFT to be real is schematically illustrated in Fig. 1. The MC-CDMA signal generation can be described as follows: user's data symbol is multiplied by different chips of a code of length $N/2-1$ generating a sequence with the same length. Then similar to performing OFDM on the coded signal, the transmitted

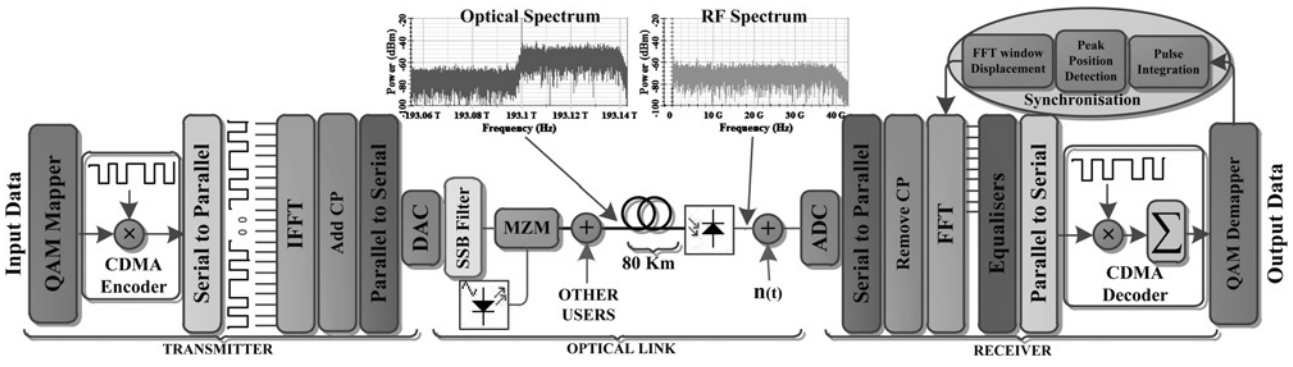

Fig. 1 *Conceptual block diagram of the proposed MC-CDMA system ((I)FFT: (inverse) fast Fourier transform, CP: cyclic prefix, DAC: digital-to-analogue converter, SSB: single side band, MZM: Mach–Zehnder modulator and ADC: analogue-to-digital converter)*

IET Optoelectron., 2015, Vol. 9, Iss. 6, pp. 325–332

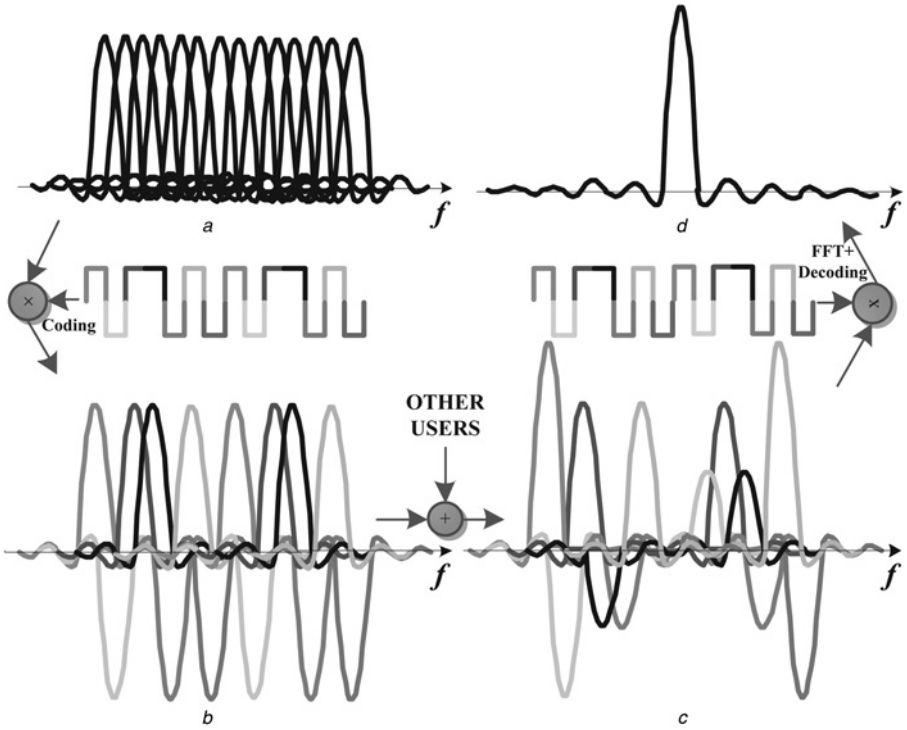

Fig. 2 *Procedure of coding and decoding in an MC-CDMA system in frequency domain*

a OFDM subcarriers
b Coded subcarriers
c Multiuser effect
d Detected signal

signal corresponding to the kth data bit of the mth user ($a_m[k]$) is

$$s_m(t) = \sum_{i=1}^{N/2-1} c_m[i]a_m[k]\mathrm{e}^{\mathrm{j}2\pi(f_c+(i/NT))t}P_T(t) \qquad c_m[i] \in \{-1,\ 1\} \tag{1}$$

where $c_m[0]$, $c_m[1]$, …, $c_m[N/2-1]$ represents the spreading code of the mth user which is a Gold sequence, f_c is the optical carrier frequency and $P_T(t)$ is unit amplitude pulse which is non-zero only in the interval of $[0, T]$; hence, T is the OFDM symbol duration. The input data symbols, $a_m[k]$, are assumed to take on values of $x+\mathrm{j}y$ in a QAM constellation where $j=\sqrt{-1}$ is the imaginary operator, and each constellation point has equal probability. Suppose that the optical fibre link has a transfer function $h_{m,i}=\rho_{m,i}\mathrm{e}^{\mathrm{j}\theta_{m,i}}$, in the mth user and the ith subcarrier. The photo-detector response of an intensity modulated/direct detection (IM/DD) system is assumed to be linear and can be represented by [21]

$$r(t) = \rho' P_0 z(t) + n(t) \tag{2}$$

where ρ' is the optical receiver responsivity, P_0 is the average received optical power, $z(t)$ is the received signal at the photo-detector and $n(t)$ is Gaussian noise introduced by photo-detector which is compound of thermal and shot noise. Consequently, $n(t)$ is given by

$$n(t) = n_{\text{shot}}(t) + n_{\text{thermal}}(t) \tag{3}$$

Now, two simplifications are used as follows: first, without loss of generality, the term $\rho' P_0$ can be inserted in $\rho_{m,i}$. Second, frequency-dependent loss is negligible which results to $\rho_{m,i}$ being independent to the subcarrier index i. Hence, the channel and photo-detector response will reduce to $\rho' P_0 h_{m,i} = \rho_m \mathrm{e}^{-\mathrm{j}\theta_{m,i}}$.

Therefore, in M active transmitters scenario, the received signal is

$$r(t) = \sum_{m=0}^{M-1}\sum_{i=1}^{N/2-1} \rho_m c_m[i]a_m[k]\mathrm{e}^{\mathrm{j}(2\pi(f_c+(i/N))(t-\tau_m)+\theta_{m,i})} \times P_T(t-\tau_m) + n(t) \tag{4}$$

where τ_m is a uniform random variable in $[0, T]$ which represents the random time delay of interfering users according to the desired users. We assume that the receiver is designed to receive the first user's data ($m=0$). After obtaining the FFT of the received signal, applying match filter and equalisation at the receiver, the signal is decoded using the 0th user code, thus for the kth bit, assuming perfect time synchronisation for the desired user's signal ($\tau_0=0$), the decision variable for this user is

$$\begin{aligned} R_0 &= \frac{1}{T}\int_0^T r(t)\ \frac{2}{N}\sum_{l=1}^{N/2-1}\left[c_0[l]\mathrm{e}^{-j2\pi(f_c+(l/NT))t}\frac{1}{\rho_0}\mathrm{e}^{-\mathrm{j}\theta_{0,i}}\right]\mathrm{d}t \\ &= \frac{2}{N}\sum_{l=1}^{N/2-1}\sum_{i=1}^{N/2-1}\sum_{m=0}^{M-1}\left[\frac{1}{T}\int_0^T\left(\frac{\rho_m}{\rho_0}c_m[i]c_0[l]a_m[k]\right.\right. \\ &\quad \left.\times \mathrm{e}^{\mathrm{j}(2\pi(f_c+(i/NT))(t-\tau_m)+(\theta_{m,ji}-\theta_{0,ji}))}P_T(t-\tau_m)+n(t)\right) \\ &\quad \left.\times\mathrm{e}^{-\mathrm{j}2\pi(f_c+(l/NT))t}\mathrm{d}t\right] \end{aligned} \tag{5}$$

where $(1/\rho_0)\mathrm{e}^{-\mathrm{j}\theta_{0,i}}$ shows the equalisation procedure. Considering ρ_m slightly varying among different users and the fact that multiplying the signal by $\mathrm{e}^{-\mathrm{j}(2\pi(f_c+(l/NT))t+\theta_{0,i})}$ does not change the complex Gaussian noise statistics, R_0 can be defined as

$$R_0 = D + I + J + \eta \tag{6}$$

where η is the corresponding noise term, I is the intra-carrier interference term and J is the inter-carrier interference that will be discussed later. D is the desired signal which is calculated by selecting $m=0$ and $l=i$ in R_0. Thus, it is calculated as follows

$$D=\frac{2}{N}\sum_{i=1}^{N/2-1}\left[\frac{1}{T}\int_0^T (c_0[i])^2 a_0[k]\mathrm{d}t\right]=a_0[k] \tag{7}$$

and the energy of the desired signal, $E(|D|^2)$ can be calculated as

$$E(|D|^2)=E\{a_0[k]a_0^*[k]\}=E_a \tag{8}$$

Intra-carrier interference from other users is achieved by selecting $m\neq 0$ and $l=i$ in R_0. Consequently, I is given by

$$\begin{aligned}I=&\frac{2}{N}\sum_{i=1}^{N/2-1}\sum_{m=1}^{M-1}\left[\frac{\rho_m}{\rho_0}c_m[i]c_1[i]\frac{1}{T}\left(\int_0^{\tau_m} a_m[k-1]\right.\right.\\&\times \mathrm{e}^{\mathrm{j}(2\pi(f_c+(i/NT))(t-\tau_m)+(\theta_{m,i}-\theta_{0,i}))}\mathrm{e}^{-\mathrm{j}2\pi(f_c+(i/NT))t}\,\mathrm{d}t\\&\left.\left.+\int_{\tau_m}^T a_m[k]\mathrm{e}^{\mathrm{j}(2\pi(f_c+(i/NT))(t-\tau_m)+(\theta_{m,i}-\theta_{0,i}))}\mathrm{e}^{-\mathrm{j}2\pi(f_c+(i/NT))t}\,\mathrm{d}t\right)\right]\\=&\frac{2}{N}\sum_{i=1}^{N/2-1}\sum_{m=1}^{M-1}\left[c_m[i]c_1[i]\frac{\rho_m}{\rho_0}\mathrm{e}^{\mathrm{j}(\theta_{m,i}-\theta_{0,i})}\left(\frac{\tau_m}{T}a_m[k-1].\right.\right.\\&\left.\left.+\left(1-\frac{\tau_m}{T}\right)a_m[k]\right)\mathrm{e}^{-\mathrm{j}2\pi(f_c+(i/NT))\tau_m}\right]\end{aligned} \tag{9}$$

where $\theta_{m,i}$ is a uniform random variable in $[0, 2\pi]$, $\rho_m=\rho' P_0\mathrm{e}^{-\alpha L_m}$, in which L_m is a uniform random variable in $[L_{\min}, L_{\max}]$, the minimum and maximum fibre lengths and $a_m[k]$ is a random variable that takes any point of the QAM constellations with equal probability. Inter-carrier interference from other users is achieved by selecting $m\neq 0$ and $l\neq i$ in R_0; hence, J is given by

$$\begin{aligned}J=&\frac{2}{N}\sum_{\substack{l=1\\l\neq i}}^{N/2-1}\sum_{i=1}^{N/2-1}\sum_{m=1}^{M-1}\left[\frac{\rho_m}{\rho_0}c_m[i]c_1[l]\frac{1}{T}\left(\int_0^{\tau_m} a_m[k-1]\right.\right.\\&\times \mathrm{e}^{\mathrm{j}(2\pi(f_c+(i/NT))(t-\tau_m)+(\theta_{m,i}-\theta_{0,i}))}\mathrm{e}^{-\mathrm{j}2\pi(f_c+(l/NT))t}\,\mathrm{d}t\\&\left.\left.+\int_{\tau_m}^T a_m[k]\mathrm{e}^{\mathrm{j}(2\pi(f_c+(i/NT))(t-\tau_m)+(\theta_{m,i}-\theta_{0,i}))}\mathrm{e}^{-\mathrm{j}2\pi(f_c+(l/NT))t}\,\mathrm{d}t\right)\right]\\=&\frac{2}{N}\sum_{\substack{l=1\\l\neq i}}^{N/2-1}\sum_{i=1}^{N/2-1}\sum_{m=1}^{M-1}\left[c_m[i]c_1[l]\frac{\rho_m}{\rho_0}\mathrm{e}^{\mathrm{j}(\theta_{m,i}-\theta_{0,i})}\right.\\&\times\left(a_m[k-1]\frac{1}{T}\int_0^{\tau_m}\mathrm{e}^{-\mathrm{j}2\pi(i-l/NT)t}\,\mathrm{d}t\right.\\&\left.\left.+a_m[k]\frac{1}{T}\int_{\tau_m}^T\mathrm{e}^{-\mathrm{j}2\pi(i-l/NT)t}\mathrm{d}t\right)\mathrm{e}^{-\mathrm{j}2\pi(f_c+(i/NT))\tau_m}\right]\\=&\frac{2}{N}\sum_{\substack{l=1\\l\neq i}}^{N/2-1}\sum_{i=1}^{N/2-1}\sum_{m=1}^{M-1}\left[c_m[i]c_1[l]\frac{\rho_m}{\rho_0}\mathrm{e}^{\mathrm{j}(\theta_{m,i}-\theta_{0,i})}\right.\\&\times\left(a_m[k-1]\frac{N}{\pi(i-l)}\mathrm{e}^{-\mathrm{j}\pi(i-l/NT)\tau_m}\sin\left(\pi\left(\frac{i-l}{NT}\right)\tau_m\right)\right.\\&\left.\left.+a_m[k]\frac{N}{\pi(i-l)}\mathrm{e}^{-\mathrm{j}\pi(i-l/NT)(T+\tau_m)}\sin\left(\pi\left(\frac{i-l}{NT}\right)(T-\tau_m)\right)\right)\right.\\&\left.\times\mathrm{e}^{-\mathrm{j}2\pi(f_c+(i/NT))\tau_m}\right]\end{aligned} \tag{10}$$

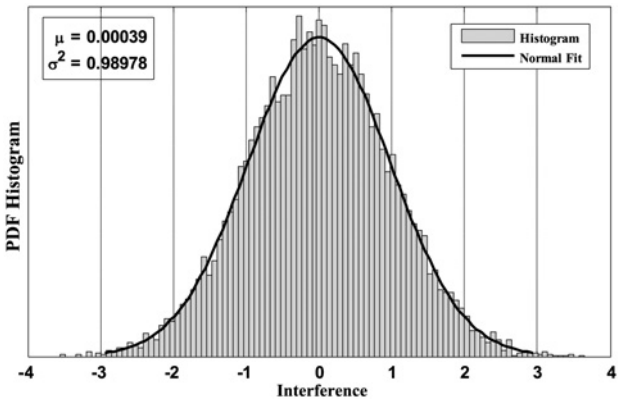

Fig. 3 *PDF histogram of the interference term real part from mathematical analysis, which is approximately Gaussian with zero mean and variances = 1 in real and imaginary parts*

Probability density function (PDF) of the interference terms ($I+J$) is represented in Fig. 3. In this figure, a normal curve is fitted to the PDF histogram of the real part of the interference terms that shows it matches with the Gaussian approximation greatly. It is worthy to note that the imaginary part has exactly the same characteristics as the real part. After some mathematical manipulation it can be deduced that the interference terms I and J have variances (see Appendixes 1 and 2, respectively)

$$\sigma_I^2=\frac{2(M-1)}{N}(\mathrm{e}^{2\alpha L_0})\left(\frac{\mathrm{e}^{-2\alpha L_{\min}}-\mathrm{e}^{-2\alpha L_{\max}}}{2\alpha(L_{\max}-L_{\min})}\right)\left(\frac{2}{3}\right)E_a \tag{11}$$

$$\sigma_J^2=\frac{4(M-1)}{N^2}(\mathrm{e}^{2\alpha L_0})\left(\frac{\mathrm{e}^{-2\alpha L_{\min}}-\mathrm{e}^{-2\alpha L_{\max}}}{2\alpha(L_{\max}-L_{\min})}\right)E_a f(N) \tag{12}$$

where $f(N)$ is defined in Appendix 2 as (26). Fig. 3 is plotted for the 4-QAM scenario considering $N=4096$ and $M=2047$ (the Gold sequence is created by an 11 digit shift register, creating codes with length $2^{11}-1=2047$) and $L_{\max}\simeq L_{\min}$. Using the same parameters in calculating σ_I^2 and σ_J^2 with the above formula we obtain $\sigma_I^2=1.3222$ and $\sigma_J^2=0.6632$. Therefore $\sigma_I^2+\sigma_J^2=1.9854$, which is a fairly good approximation for the amount, $\sigma_I^2=0.98978\times 2=1.9796$, which is reached in simulations (2 is multiplied to consider both real and imaginary parts which are identical).

The noise term $\eta=\eta_{\text{shot}}+\eta_{\text{thermal}}$ is Gaussian with zero mean and variances of $S_{\text{th}}^2\Delta f+2q\rho' P_0\Delta f$, where S_{th} is the thermal noise density, Δf is the receiver bandwidth and q is the electron charge [28]. Hence, the system signal-to-interference plus noise ratio (SINR) is defined by

$$\begin{aligned}\text{SINR}&=\frac{E(|D|^2)}{\text{var}(I)+\text{var}(J)+\text{var}(\eta)}\\&=\frac{E_a}{\sigma_I^2+\sigma_J^2+S_{\text{th}}^2\Delta f+2q\rho' P_0\Delta f}\end{aligned} \tag{13}$$

The system performance can now be easily evaluated using well-known results for the system BER evaluation. For instance, in the case of rectangular QAM the system BER is evaluated using

the following expression [29]

$$\mathrm{BER}_{P.\mathrm{QAM}} = \frac{2}{\log_2 P}\left(1 - \frac{1}{\sqrt{P}}\right) Q\left(\sqrt{\frac{3\,\mathrm{SINR}}{2(P-1)}}\right)$$
$$= \frac{2}{\log_2 P}\left(1 - \frac{1}{\sqrt{P}}\right) \times Q\left(\sqrt{\frac{3E_a}{2(P-1)(\sigma_I^2 + \sigma_J^2 + S_{\mathrm{th}}^2 \Delta f + 2q\rho' P_0 \Delta f')}}\right) \quad (14)$$

in which erfc(x) is defined as follows

$$Q(x) = \frac{1}{\sqrt{2\pi}} \int_x^{\infty} \mathrm{e}^{-(t^2/2)}\,\mathrm{d}t \quad (15)$$

4 PAPR reduction

Talking about OFDM-based systems, one could never escape the challenges caused by high PAPR. In general, the PAPR for an OFDM symbol is given as follows

$$\mathrm{PAPR} = \frac{\max\limits_{1 \le n \le N} \{|x_n|^2\}}{\mathrm{mean}\{|x_n|^2\}} \quad (16)$$

where $\{x_n\}$ is the output sequence of the transmitter IFFT. MC-CDMA systems have better PAPR from conventional OFDM systems with the same parameters. This is due to the fact that the FFT inputs are the codes which do not have the wide selection of input ranges. For example, here there are N codes instead of 2^N data symbols [21]; this can be seen in Fig. 4 which compares conventional OFDM with the proposed MC-CDMA in terms of probability of PAPR being more than a particular amount. Generally, a conventional OFDM with N available subcarriers has 2^N input selection which leads to different PAPRs. Obviously, in conventional OFDM, one per cent of the PAPRs are more than 10.9 dB, whereas in MC-CDMA only one per cent of PAPRs exceeds 10.3 dB. Although the proposed MC-CDMA has lower PAPR compared with conventional OFDM systems, we propose a simple method to reduce PAPR even more.

Suppose there is a matrix containing all Gold sequence codes, where each row of the matrix is a Gold sequence. Each row can be used as the input of the available subcarriers in transmitter IFFT of the proposed MC-CDMA system and the PAPR is calculated at the transmitter output. Then, by considering this information, the rows of the Gold sequence code matrix are sorted based on the calculated PAPR in ascending order. In a dynamic code assignment system, this sorted matrix can be used to assign codes to different users in an ascending order or if the codes are assigned to users statically, codes with lower PAPR can be assigned to users with more traffic and a few codes with very high PAPR can be unused. As illustrated in Fig. 4, 75% of the codes have PAPR <9 dB which are very good for such a long FFT size. In 1% of the codes, the PAPR is more than 10.3 dB, which can be unused to avoid high PAPR.

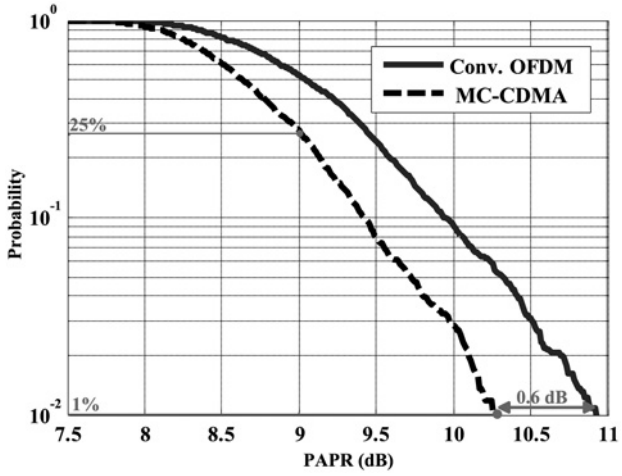

Fig. 4 *PAPR comparisons of conventional OFDM with the proposed MC-CDMA in terms of probability of PAPR being more than a particular amount*

5 Simulations and results

5.1 Simulation structure

Numerical simulations were conducted using OptiSystem for the optical link and MATLAB for implementing the transmitter and receiver. The IM/DD optical MC-CDMA transmitter uses a 4096-point IFFT. OFDM symbols are generated in MATLAB and used in OptiSystem to drive the MZM. Each subcarrier has 20 MHz bandwidth which leads to total bandwidth of 40 GHz in single side. The optical link comprises 80 km of SSMF which has an attenuation of 0.2 dB/km, dispersion of 17 ps/nm/km and a non-linearity factor of 1.3 km^{-1} W^{-1}. After detection, the received signal is equalised and the BER is calculated in MATLAB. In this paper, Gold sequences with length of 2047 are used for coding and decoding. In 16-QAM senario, each user has a bit rate equal to 80 Mb/s and the CP ratio is 1/8. The simulation parameters are summarised in Table 1. It is necessary to mention that for each user the BER is calculated individually and then to have a more accurate and unbiased performance evaluation and to increase the accuracy the BER curves averaging over the BER of all active users are performed. It is worthy to note to mention that since this design is scalable we can easily change the size of FFT and users code to scale for different bandwidths. The block diagram of the transmitter, channel and receiver is shown in Fig. 1.

5.2 Simulation results

Fig. 5 compares analytical and simulation results of BER performance against the number of users for three different modulation formats after 80 km of SSMF in $E_b/N_0 = 15$ dB. The closeness between analytical and simulation results validates the accuracy of the presented mathematical modelling. Furthermore, from the results we can observe that in higher modulation level, fewer users are allowed to achieve a desired BER performance. In Fig. 5, the forward error correction (FEC) limit, that is, 3×10^{-3}, is shown by horizontal line. Considering this limit, one can see that about 256, 128 and 50 simultaneous users are allowed in 4-QAM, 8-QAM and 16-QAM modulation formats, respectively.

Table 1 Simulation parameters

Quantity	Value
FFT/IFFT size	4096
subcarrier bandwidth	20 MHz
total bandwidth	40 GHz
SSMF length	80 km
SSMF attenuation	0.2 dB/km
SSMF dispersion	17 ps/nm/km
background light current (I_b)	202 μA
noise density (N_0)	$2qI_b$
detector area (A_{det})	1 cm^2
absolute temperature (T)	295 K
Boltzmann constant (k)	1.23×10^{-23}
CP ratio	1/8
Gold sequence length	2047
users bit rate (16 QAM)	80 Mb/s

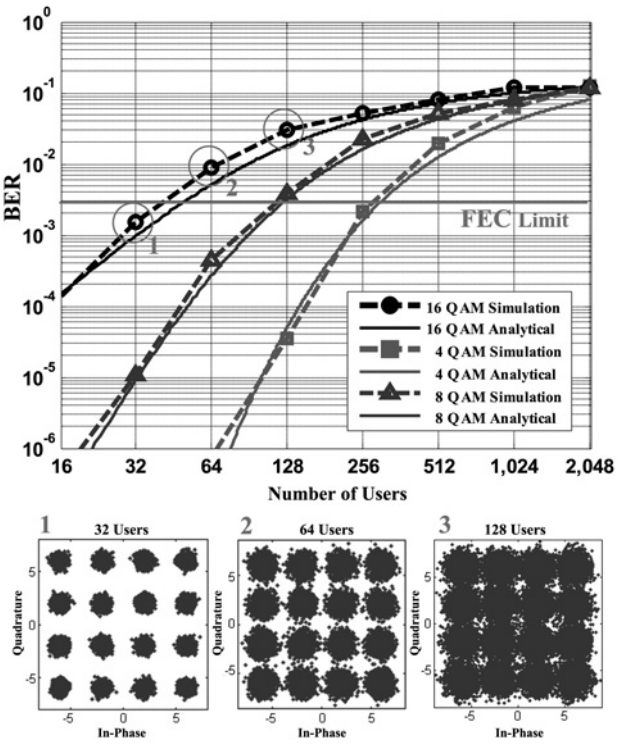

Fig. 5 *Analytical and simulation results of BER performance for the proposed MC-CDMA against number of users conditioned to different modulation formats and the corresponding equalised constellations*

This figure also compares the constellations for three different numbers of users. As the scatter-plot shows, in high number of users, different constellation points are not distinguishable which leads to higher BER.

In Fig. 6, analytical and simulation results of BER curves against E_b/N_0 for three different modulation formats and their equalised constellations are presented. This figure is plotted for 128 active users' scenario. As it can be observed, in E_b/N_0 higher than 10, 15 and 20 dB the 4-QAM, 8-QAM and 16-QAM curves drop below the FEC limit, respectively. As the modulation level is increased, because of a higher spectral efficiency, the bit rate is also increased, whereas the performance is degraded. Choosing appropriate values for M, L and N enables obtaining the required bit rate, BER and other specifications for different users in the network. It is worthy to note to mention that these parameters can be chosen dynamically for most efficient performance. For example, based on the required bit rates, different users of the network can employ different QAM mapping.

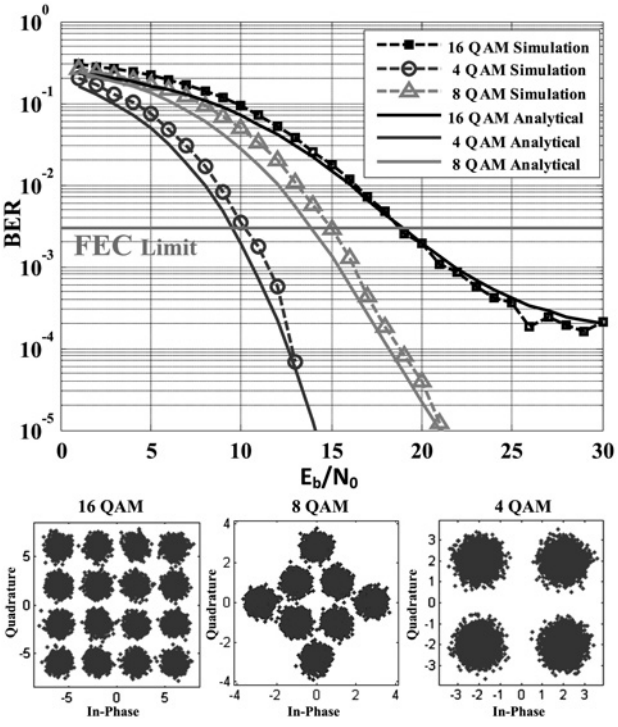

Fig. 6 *Analytical and simulation results of BER performance against E_b/N_0 conditioned on different modulation formats and the corresponding equalised constellations*

6 Conclusion

Performance of asynchronous MC-CDMA for IM/DD systems used in next-generation optical long-reach access networks was evaluated. It was shown that the proposed MC-CDMA system takes the advantages of the dense subcarrier spacing of OFDM and the multiple access benefits of CDMA. Mathematical formulations for the proposed system were derived and closed-form equations for the SINR and BER performances were obtained. Furthermore, the simulation results were provided in terms of BER against signal-to-noise ratio in one case and the number of users in another, conditioned on the modulation levels. Finally, the analytical formulation of BER was verified with the help of simulation results. It was shown that in the proposed system employing 80 km SSMF can support up to 256 asynchronous users and PAPR is reduced more than 0.6 dB.

7 References

1 Qian, D., Cvijetic, N., Hu, J., Wang, T.: 'Optical OFDM transmission in metro/access networks'. Optical Fiber Communication Conf., Optical Society of America, 2009

2 Cvijetic, N.: 'OFDM for next-generation optical access networks', *IEEE J. Lightwave Technol.*, 2012, **30**, (4), pp. 384–398

3 Shoreh, M.H.: 'Compensation of nonlinearity impairments in coherent optical OFDM systems using multiple optical phase conjugate modules', *J. Opt. Commun. Netw.*, 2014, **6**, (6), pp. 549–558

4 Shoreh, M.H., Beyranvand, H., Salehi, J.A.: 'Mathematical modeling of nonlinearity impairments in optical OFDM communication systems using multiple optical phase conjugate'. Iran Workshop on Communication and Information Theory (IWCIT), 2013, pp. 1–5

5 Christodoulopoulos, K., Tomkos, I., Varvarigos, E.A.: 'Elastic bandwidth allocation in flexible OFDM-based optical networks', *IEEE J. Lightwave Technol.*, 2011, **29**, (9), pp. 1354–1366

6 Armstrong, J.: 'OFDM for optical communications', *IEEE J. Lightwave Technol.*, 2009, **27**, (3), pp. 189–204

7 Shieh, W., Djordjevic, I.: 'OFDM for optical communications' (Academic Press, 2009)

8 Ghanaatian, R., Shabany, M., Shoreh, M.H.: 'A high-throughput VLSI architecture for real-time optical OFDM systems with an efficient phase equalizer', *Can. J. Electr. Comput. Eng.*, 2014, **37**, (2), pp. 86–93

9 Qian, D., Hu, J., Yu, J. *et al.*: 'Experimental demonstration of a novel OFDM-A based 10 Gb/s PON architecture', *ECOC 2007*, **2007**, pp. 1–2

10 Liang, C., Krongold, B., Evans, J.: 'Performance analysis for optical OFDM transmission in short-range IM/DD systems', *IEEE J. Lightwave Technol.*, 2012, **30**, pp. 974–983

11 Hanzo, L., Munster, M., Choi, B.J., Keller, T.: 'OFDM and MC-CDMA for broadband multiuser communications, WLANs and broadcasting' (Wiley-IEEE Press, New York, 2003)

12 Armstrong, J., Schmidt, B.J.C., Kalra, D., Suraweera, H.A., Lowery, A.J.: 'Performance of asymmetrically clipped optical OFDM in AWGN for an intensity modulated direct detection system'. Proc. IEEE Global Telecommunications Conf., 2006, pp. 1–5

13 Jin, X.Q., Giddings, R.P., Hugues-Salas, E., Wei, J.L., Groenewald, J., Tang, J.M.: 'First real-time experimental demonstrations of 11.25 Gb/s optical OFDMA PONs with adaptive dynamic bandwidth allocation', *Opt. Express*, 2011, **19**, (21), pp. 20 557–20 570

14 Salehi, J.A.: 'Code division multiple-access techniques in optical fiber networks – part I: fundamental principles', *IEEE Trans. Commun.*, 1989, **37**, pp. 824–833

15 Ottosson, T., Svensson, A.: 'Multi-rate performance in DS/CDMA system'. Technical Report, no. 14, Department of Information Theory, Charlmers University of Technology, Goteborg, Sweden, March 1995, ISSN 0283-1260

16 Willner, A.E., Saghari, P., Arbab, V.R.: 'Advanced techniques to increase the number of users and bit rate in OCDMA networks', *IEEE J. Sel. Top. Quantum Electron.*, 2007, **13**, (5), pp. 1403–1414

IET Optoelectron., 2015, Vol. 9, Iss. 6, pp. 325–332

17 Chung, F.R., Salehi, J.A., Wei, V.K.: 'Optical orthogonal codes: design, analysis and applications', *IEEE Trans. Inf. Theory*, 1989, **35**, (3), pp. 595–604
18 Arbab, V.R., Peng, W.-R., Wu, X., Willner, A.E.: 'Experimental demonstration of multicarrier-CDMA for passive optical networks'. 34th European Conf. on Optical Communication, 2008, pp. 1–2
19 Hara, S., Prasad, R.: 'Overview of multicarrier CDMA', *IEEE Commun. Mag.*, 1997, **35**, (12), pp. 126–133
20 Hanzo, L.L., Keller, T.: 'OFDM and MC-CDMA: a primer' (John Wiley & Sons, 2007)
21 You, Y.-H., Jeon, W.-G., Paik, J.-H., Song, H.-K.: 'A simple construction of OFDM-CDMA signals with low peak-to-average power ratio', *IEEE Trans. Broadcast.*, 2003, **49**, pp. 403–407
22 van de Beek, J.-J., Brjesson, P.O., Boucheret, M.-L., *et al.*: 'A time and frequency synchronization scheme for multiuser OFDM', *IEEE J. Sel. Areas Commun.*, 1999, **17**, pp. 1900–1914
23 Kaiser, S.: 'OFDM-CDMA versus DS-CDMA: performance evaluation for fading channels'. Proc. IEEE Int. Conf. Communication (ICC'95), June 1995, pp. 1722–1726
24 Fu, P.-W., Chen, K.-C.: 'A programmable transceiver structure of multi-rate OFDM-CDMA for wireless multimedia communications'. IEEE VTS 53rd Vehicular Technology Conf., 2001, vol. 3, pp. 1942–1946
25 Chen, J.-D., Ueng, F.-B., Chang, J.-C., Su, H.: 'Performance analyses of OFDM-CDMA receivers in multipath fading channels', *IEEE Trans. Veh. Technol.*, 2009, **58**, (9), pp. 4805–4818
26 Kim, P.K., Oh, S.K.: 'An OFDM-CDMA scheme using orthogonal code multiplexing and its parallel interference cancellation receiver'. IEEE ISSSTA, Czech Report, September 2002, pp. 368–372
27 Shoreh, M.H., Hosseinianfar, H., Akhoundi, F., Yazdian, E., Farhang, M., Salehi, J.A.: 'Design and implementation of spectrally-encoded spread-time CDMA transceiver', *IEEE Commun. Lett.*, 2014, **18**, (5), pp. 741–744
28 Vanin, E.: 'Performance evaluation of intensity modulated optical OFDM system with digital baseband distortion', *Opt. Express*, 2011, **19**, (5), pp. 4280–4293
29 Vitthaladevuni, P.K., Alouini, M.-S., Kieffer, J.C.: 'Exact BER computation for cross QAM constellations', *IEEE Trans. Wirel. Commun.*, 2005, **4**, (6), pp. 3039–3050

8 Appendix

8.1 Appendix 1: Intra-carrier interference variances calculations

In this appendix, we derive a closed-form formulation for the intra-carrier interference variances. From (9), we obtain

$$\begin{aligned} II^* = \frac{4}{N^2}\sum_{i'=1}^{N/2-1}\sum_{m'=1}^{M-1}\sum_{i=1}^{N/2-1}\sum_{m=1}^{M-1}\Bigg[& c_m[i]c_1[i]c_{m'}[i']c_1[i']\frac{\rho_m\rho_{m'}}{\rho_0^2} \\ & \times \mathrm{e}^{\mathrm{j}(\theta_{m,i}-\theta_{m',i'})}\left(\frac{\tau_m}{T}a_m[k-1]+\left(1-\frac{\tau_m}{T}\right)a_m[k]\right) \\ & \times \left(\frac{\tau_{m'}}{T}a_{m'}[k-1]+\left(1-\frac{\tau_{m'}}{T}\right)a_{m'}[k]\right) \\ & \times \mathrm{e}^{-\mathrm{j}2\pi(f_c+(i/NT))\tau_m}\mathrm{e}^{+\mathrm{j}2\pi(f_c+(i'/NT))\tau_{m'}}\Bigg] \end{aligned} \tag{17}$$

Since $E\{I\}=0$ in order to calculate σ_I^2 we should calculate the average of II^*, thus

$$\begin{aligned} \sigma_I^2 = E\{II^*\} = \frac{4}{N^2}\sum_{i'=1}^{N/2-1}\sum_{m'=1}^{M-1}\sum_{i=1}^{N/2-1}\sum_{m=1}^{M-1}\Bigg[& c_m[i]c_1[i]c_{m'}[i']c_1[i'] \\ & \times E\left\{\frac{\rho_m\rho_{m'}}{\rho_0^2}\right\}E\left\{\mathrm{e}^{\mathrm{j}(\theta_{m,i}-\theta_{m',i'})}\right\} \\ & \times E_{a_m}E_{\tau_m}\Bigg\{\Bigg\{\Bigg(a_m[k-1]a_{m'}[k-1]\frac{\tau_m\tau_{m'}}{T^2} \\ & + a_m[k]a_{m'}[k]\left(1-\frac{\tau_m}{T}\right)\left(1-\frac{\tau_{m'}}{T}\right) \\ & + a_m[k-1]a_{m'}[k]\frac{\tau_m}{T}\left(1-\frac{\tau_{m'}}{T}\right) \\ & + a_m[k]a_{m'}[k-1]\left(1-\frac{\tau_m}{T}\right)\frac{\tau_{m'}}{T}\Bigg) \\ & \times \mathrm{e}^{-\mathrm{j}2\pi(f_c+(i/NT))\tau_m}\mathrm{e}^{\mathrm{j}2\pi(f_c+(i'/NT))\tau_{m'}}\Bigg\}\Bigg\}\Bigg] \end{aligned} \tag{18}$$

where E_{a_m} and E_{τ_m} states that the averaging is performed on a_m and τ_m, respectively. Considering the fact that for $a_m[k]$ being a random point of a QAM constellation where each point has equal probability, because of symmetrical cancellation $E\{a_m[k]a_{m'}[k']\}\neq 0$ only if $m=m'$ and $k=k'$, we can obtain $E\{a_m[k-1]a_{m'}[k-1]\}=E\{a_m[k]a_{m'}[k]\}=\delta[m-m']E_a$ and $E\{a_m[k-1]a_{m'}[k]\}=E\{a_m[k]a_{m'}[k-1]\}=0$, resulting in $m=m'$ in (18); hence, $E\{\mathrm{e}^{\mathrm{j}(\theta_{m,i}-\theta_{m,i'})}\}=\delta[i-i']$, $E\left\{\frac{\rho_m\rho_{m'}}{\rho_0^2}\right\}=\overline{\frac{\rho_m^2}{\rho_0^2}}$ and $(c_1[i])^2=1$. By replacing that in (18), it simplifies to

$$\begin{aligned} \sigma_I^2 &= \frac{4}{N^2}\sum_{i=1}^{N/2-1}\sum_{m=1}^{M-1}\left[\overline{\frac{\rho_m^2}{\rho_0^2}}E_aE\left\{\frac{\tau_m^2}{T^2}+\left(1-\frac{\tau_m}{T}\right)^2\right\}\right] \\ &= \frac{4}{N^2}\frac{1}{T^2}\sum_{i=1}^{N/2-1}\sum_{m=1}^{M-1}\left[\overline{\frac{\rho_m^2}{\rho_0^2}}E_a\frac{1}{T}\int_0^T(2\tau_m^2+T^2-2T\tau_m)\mathrm{d}\tau_m\right] \\ &= \frac{4}{N^2}\sum_{i=1}^{N/2-1}\sum_{m=1}^{M-1}\left[\overline{\frac{\rho_m^2}{\rho_0^2}}E_a\left(\frac{2}{3}\right)\right] = \frac{2(M-1)}{N}\left(\frac{2}{3}\right)\overline{\frac{\rho_m^2}{\rho_0^2}}E_a \end{aligned} \tag{19}$$

where

$$\begin{aligned} \overline{\frac{\rho_m^2}{\rho_0^2}} &= E\left\{\overline{\frac{\rho_m^2}{\rho_0^2}}\right\} = E\left\{\frac{(\rho' P_0)^2\mathrm{e}^{-2\alpha L_m}}{(\rho' P_0)^2\mathrm{e}^{-2\alpha L_0}}\right\} \\ &= \frac{\mathrm{e}^{2\alpha L_0}}{L_{\max}-L_{\min}}\int_{L_{\min}}^{L_{\max}}\mathrm{e}^{-2\alpha L_m}\mathrm{d}l_m \\ &= (\mathrm{e}^{2\alpha L_0})\left(\frac{\mathrm{e}^{-2\alpha L_{\min}}-\mathrm{e}^{-2\alpha L_{\max}}}{2\alpha(L_{\max}-L_{\min})}\right) \end{aligned} \tag{20}$$

inserting (20) in (19), finally, the closed form for σ_I^2 is calculated as follows

$$\sigma_I^2 = \frac{2(M-1)}{N}(\mathrm{e}^{2\alpha L_0})\left(\frac{\mathrm{e}^{-2\alpha L_{\min}}-\mathrm{e}^{-2\alpha L_{\max}}}{2\alpha(L_{\max}-L_{\min})}\right)\left(\frac{2}{3}\right)E_a \tag{21}$$

8.2 Appendix 2: Inter-carrier interference variances calculations

In this appendix, we derive a closed-form formulation for the inter-carrier interference variances. From (10) we obtain

$$\begin{aligned} JJ^* = \frac{4}{N^2}\sum_{\substack{l'=1\\ l'\neq i'}}^{N/2-1}\sum_{i'=1}^{N/2-1}\sum_{m'=1}^{M-1}\sum_{\substack{l'=1\\ l'\neq i'}}^{N/2-1}\sum_{i=1}^{N/2-1}\sum_{m=1}^{M-1}\Bigg[& c_m[i]c_1[l]c_{m'}[i']c_1[l']\frac{\rho_m\rho_{m'}}{\rho_0^2} \\ & \times \mathrm{e}^{\mathrm{j}(\theta_{m,i}-\theta_{m',i'})}\Bigg(a_m[k-1]\frac{N}{\pi(i-l)}\mathrm{e}^{-\mathrm{j}\pi(i-l/NT)\tau_m}\sin\left(\pi\left(\frac{i-l}{NT}\right)\tau_m\right) \\ & + a_m[k]\frac{N}{\pi(i-l)}\mathrm{e}^{-\mathrm{j}\pi(i-l/NT)(T+\tau_m)}\sin\left(\pi\left(\frac{i-l}{NT}\right)(T-\tau_m)\right)\Bigg) \\ & \times \left(a_{m'}[k-1]\frac{N}{\pi(i'-l')}\mathrm{e}^{-\mathrm{j}\pi(i'-l'/NT)\tau'_m}\sin\left(\pi\left(\frac{i'-l'}{NT}\right)\tau'_m\right)\right. \\ & \left.+a_{m'}[k]\frac{N}{\pi(i'-l')}\mathrm{e}^{-\mathrm{j}\pi(i'-l'/NT)(T+\tau'_m)}\sin\left(\pi\left(\frac{i'-l'}{NT}\right)(T-\tau'_m)\right)\right) \\ & \times \mathrm{e}^{-\mathrm{j}2\pi(f_c+(i/NT))\tau_m}\mathrm{e}^{+\mathrm{j}2\pi(f_c+(i'/NT))\tau_{m'}}\Bigg] \end{aligned} \tag{22}$$

Considering the fact that $E\{J\}=0$, to calculate σ_J^2 the average of JJ^* should be calculated. For the same reasons as discussed in Appendix

1, $m=m'$, $i=i'$, $E\left\{\frac{\rho_m\rho_{m'}}{\rho_0^2}\right\}=\frac{\overline{\rho_m\rho_{m'}}}{\rho_0^2}$ and $(c_m[i])^2=1$, thus

$$\begin{aligned}\sigma_J^2 &= E\{JJ^*\}\\ &= \frac{4}{N^2}\sum_{\substack{l'=1\\ l'\neq i'}}^{N/2-1}\sum_{\substack{l'=1\\ l'\neq i'}}^{N/2-1}\sum_{i=1}^{N/2-1}\sum_{m=1}^{M-1}\left[\frac{\overline{\rho_m^2}}{\rho_0^2}c_1[l]c_1[l']E_a\right.\\ &\quad\times E_{\tau_m}\left\{\left(\frac{N}{\pi(i-l)}\mathrm{e}^{-\mathrm{j}\pi(i-l/NT)\tau_m}\sin\left(\pi\left(\frac{i-l}{NT}\right)\tau_m\right)\right)\right.\\ &\quad\times\left(\frac{N}{\pi(i^-l')}\mathrm{e}^{-\mathrm{j}\pi(i-l'/NT)\tau_m}\sin\left(\pi\left(\frac{i-l'}{NT}\right)\tau_m\right)\right)\\ &\quad+\left(\frac{N}{\pi(i-l)}\mathrm{e}^{-\mathrm{j}\pi(i-l/NT)(T+\tau_m)}\sin\left(\pi\left(\frac{i-l}{NT}\right)(T-\tau_m)\right)\right)\\ &\quad\left.\left.\times\left(\frac{N}{\pi(i-l')}\mathrm{e}^{-\mathrm{j}\pi(i-l'/NT)(T+\tau_m)}\sin\left(\pi\left(\frac{i-l'}{NT}\right)(T-\tau_m)\right)\right)\right\}\right]\end{aligned}\tag{23}$$

Therefore

$$\begin{aligned}\sigma_J^2 &= \frac{4}{N^2}\sum_{\substack{l'=1\\ l'\neq i'}}^{N/2-1}\sum_{\substack{l'=1\\ l'\neq i'}}^{N/2-1}\sum_{i=1}^{N/2-1}\sum_{m=1}^{M-1}\left[\frac{\overline{\rho_m^2}}{\rho_0^2}c_1[l]c_1[l']E_a\right.\\ &\quad\times\frac{N^2}{\pi^2(i-l)(i^-l')}\left\{\frac{1}{T}\int_0^T\left(\mathrm{e}^{-\mathrm{j}\pi(2i-l-l'/NT)\tau_m}\right.\right.\\ &\quad\left.\left.\times\sin\left(\pi\left(\frac{i-l}{NT}\right)\tau_m\right)\sin\left(\pi\left(\frac{i-l'}{NT}\right)\tau_m\right)\mathrm{d}\tau_m\right.\right.\\ &\quad+\frac{1}{T}\int_0^T\left(\mathrm{e}^{-\mathrm{j}\pi(2i-l-l'/NT)(T+\tau_m)}\sin\left(\pi\left(\frac{i-l}{NT}\right)(T-\tau_m)\right)\right.\\ &\quad\left.\left.\left.\times\sin\left(\pi\left(\frac{i-l'}{NT}\right)(T-\tau_m)\right)\right)\mathrm{d}\tau_m\right\}\right]\end{aligned}\tag{24}$$

after some mathematical manipulation, we obtain

$$\begin{aligned}\sigma_J^2 &= \frac{4(M-1)}{N^2}(\mathrm{e}^{2\alpha L_0})\left(\frac{\mathrm{e}^{-2\alpha L_{\min}}-\mathrm{e}^{-2\alpha L_{\max}}}{2\alpha(L_{\max}-L_{\min})}\right)E_a\\ &\quad\times\sum_{\substack{l'=1\\ l'\neq i'}}^{N/2-1}\sum_{\substack{l'=1\\ l'\neq i'}}^{N/2-1}\sum_{i=1}^{N/2-1}\left[c_1[l]c_1[l']\frac{N^2}{4\pi^2(i-l)(i^-l')}\right.\\ &\quad\left.\times\left\{-(1+\delta[2i-l-l'])(1+\mathrm{e}^{-\mathrm{j}2\pi(2i-l-l'/N)})\right\}\right]\\ &= \frac{4(M-1)}{N^2}(\mathrm{e}^{2\alpha L_0})\left(\frac{\mathrm{e}^{-2\alpha L_{\min}}-\mathrm{e}^{-2\alpha L_{\max}}}{2\alpha(L_{\max}-L_{\min})}\right)E_a f(N)\end{aligned}\tag{25}$$

where $f(N)$ is defined as follows

$$\begin{aligned}f(N) &= \sum_{\substack{l'=1\\ l'\neq i'}}^{N/2-1}\sum_{\substack{l'=1\\ l'\neq i'}}^{N/2-1}\sum_{i=1}^{N/2-1}\left[c_1[l]c_1[l']\frac{N^2}{4\pi^2(i-l)(i^-l')}\right.\\ &\quad\left.\times\left\{-(1+\delta[2i-l-l'])(1+\mathrm{e}^{-\mathrm{j}2\pi(2i-l-l'/N)})\right\}\right]\end{aligned}\tag{26}$$

IET Optoelectron., 2015, Vol. 9, Iss. 6, pp. 325–332